DOI 10.1515/aot-2013-0064 — Adv. Opt. Techn. 2014; 3(2): 161–178

Review Article

Ove Steinvall*

Active spectral imaging and mapping

Abstract: Active imaging and mapping using lasers as illumination sources have been of increasing interest during the last decades. Applications range from defense and security, remote sensing, medicine, robotics, and others. So far, these laser systems have mostly been based on a fix wavelength laser. Recent advances in lasers enable emission of tunable, multiline, or broadband emission, which together with the development of array detectors will extend the capabilities of active imaging and mapping. This paper will review some of the recent work on active imaging mainly for defense and security and remote sensing applications. A short survey of basic lidar relations and present fix wavelength laser systems is followed by a review of the benefits of adding the spectral dimension to active and/or passive electro-optical systems.

Keywords: active imaging; ladar; laser sensors; lidar; mapping; remote sensing; spectral imaging.

OCIS codes: 280.4788; 120.0280; 110.4234; 280.3640.

***Corresponding author: Ove Steinvall,** Swedish Defense Research Agency (FOI), Box 1165, Linköping, Sweden, e-mail: ove.steinvall@foi.se

1 Introduction

Active or laser-assisted imaging is an area that is gaining more and more interest in various fields such as remote sensing, defense and security, robotics, medicine, and others. Laser scanning systems, for example, are now widely spread for urban, terrain, water and seafloor mapping; creating high-resolution three-dimensional (3-D) data sets from which 'images' can be extracted for a number of civilian and military applications. Active imaging is also utilized in security and defense for target classification and identification. Range gating is usually employed to enhance the target from the foreground and background, and to suppress the daylight background, thereby, enhancing target detection and identification. Adding a multispectral or broadband laser will substantially improve the image quality by reducing the speckle noise effects and also increase the target detection and identification capability by spectral discrimination.

This paper will review some of the recent work on active imaging mainly for defense and security and remote sensing applications. Other examples of recent reviews on laser sensing have been reported by McMannamon [1], Steinvall [2], and Molebny [3, 4].

In this paper, focus will be put on new capabilities and especially to the combination of active with spectral imaging either by employing a spectrally tunable source or by combining a fixed wavelength active imager with a passive multi or hyperspectral sensor.

2 Basic relations of active imaging and mapping

An active laser-based imaging system scans or flood illuminates the area of interest. The reflected radiation from the scene is captured by the receiver, which may contain a detector array or a single detector. In general, the maximum range can be estimated from the laser radar equation, which for an angular resolved target (the beam is smaller than the target cross-section area) can be formulated as:

$$SNR_T = \frac{P_r}{NEP} = \frac{P_L \cdot \eta \cdot G \cdot A_r}{NEP \cdot R^2} \cdot \exp\left(-2\int_0^R \sigma(R')\,dR'\right) \qquad (1)$$

where P_L is the laser power, P_r is the received optical power, NEP is the noise equivalent power, η is the overall system efficiency, A_r is the receiver area, R is the target range, and σ is the atmospheric attenuation coefficient. The parameter G denotes the normalized reflected intensity, which for a diffuse Lambertian target is ρ/π , ρ being the reflectivity. We will start by assuming the attenuation is independent of range and dominated atmospheric aerosols, which simplifies the atmospheric loss term to $exp(-2\sigma R)$.

In equation (1), the assumption is that a single detector is used. For a staring system with a detector array of N^2 elements we have to adjust the laser power to that per pixel, which for an even illumination implies P_L/N^2 for the

emitted laser power. We also have to adjust the NEP to cope for the change in instantaneous field of view of the detector as the pixel size in an array generally is smaller than a single detector often used in scanning systems.

For an atmospheric lidar, the parameter G can be substituted by $G=\beta c\tau/2$, where β is the backscatter coefficient, c is the velocity of light, and τ is the laser pulse length. For the atmospheric lidar when the atmospheric loss is dominated by aerosol attenuation, we can often use the empirical relation [5] connecting the backscatter coefficient with aerosol scatter attenuation, $\beta=f(\sigma)$ according to some simple exponential or polynomial expression of the scattering attenuation σ. Similar relations have been suggested for water depth-sounding lidars relating the diffuse attenuation coefficient K to the backscatter β.

For a small unresolved target (target cross-section area smaller than the beam), the corresponding ladar equation can be written as:

$$SNR_T=\frac{P_r}{NEP}=\frac{P_L\cdot\eta\cdot G\cdot A_r}{NEP\cdot R^2}\cdot\frac{A_T\cdot 4}{\pi(R\theta)^2}\exp(-2\sigma R) \tag{2}$$

where θ is the beam divergence, and A_T is the target cross section area.

A very special type of reflector is the retroreflector, which returns the beam in the same direction independent of angle of incidence (within the acceptance angle of the device). The cross-section G^*A_T of an idealized retroreflector is

$$G\cdot A_T=kA_T/\lambda^2 \tag{3}$$

where k is a constant depending on the retroreflector geometry (trihedral, conical, etc.), and A_T is the cross-section area.

The noise equivalent power for a direct detection ladar using an avalanche photo diode (APD) detector can be written as [6]:

$$NEP=\frac{[(\overline{I_{BN}^2}+\overline{I_{DN}^2})M^2F+\overline{I_{PN}^2}]^{1/2}}{R_D M T_{opt}\eta_e} \tag{4}$$

where $\overline{I_{BN}^2}$ is the unity-gain rms background noise current (A), $\overline{I_{DN}^2}$ is the unity-gain rms detector dark noise current, $\overline{I_{PN}^2}$ is the rms preamplifier noise current, M is the photodetector gain, F is the excess noise factor, R_D is the unity-gain responsivity of the detector (A/W), T_{opt} is the receiver optical transmission, and η_e is the factor by which the peak signal is reduced due to bandwidth limitation.

The background current $\overline{I_{BN}^2}$ depends on the scattered solar irradiation and, for longer wavelength thermal emission, form the target scene. The background shot noise current at the output of the detector assuming unity gain is given by [6]

$$(\overline{I_{BN}^2})^{1/2}=(2q\cdot i_B\cdot B)^{1/2} \tag{5}$$

where q is the electronic charge (1.6×10^{-19}), i_B is the total DC background current, and B is the receiver noise bandwidth. Ignoring the atmospheric losses between the target and receiver, the DC background current i_B is given by

$$i_B=R_D\cdot A_r\cdot T_{opt}\cdot\Delta\lambda\cdot\Omega_{FOV}[E_\lambda\rho_{bcgr}/\pi+M_\lambda/\pi] \tag{6}$$

where $\Delta\lambda$ is the full-width half maximum (FWHM) optical bandpass of the receiver (μm), Ω_{FOV} is the solid angle of the receiver detector (sr), E_λ is the spectral irradiance of the sun (W/m² μm), ρ_{bcgr} is the target or background reflectivity (whichever dominates the detector FOV), and M_λ is the spectral radiant exitance of the target (W/m² μm).

The atmospheric attenuation is often dominated by aerosol losses for practical wavelengths used in practical ladar systems. The example of empirical relations for the attenuation σ relative to the meteorological visibility V is given, for example, by Hutt [7]. FOI has also studied the issue of aerosol extinction vs. wavelength [8].

We note that the solution of the ladar equations (1) and (2) can be obtained from an equation of the type

$$W\cdot\exp(W)=x \tag{7}$$

This equation has the so-called Lambert's W function as a solution [9]. For the resolved target case, we identify the solution y_1=Lambertw(x_1). where $y=\sigma R$ and

$$x_1=\sigma\sqrt{S_1}=\sigma\sqrt{\frac{\eta\cdot P_L\cdot G\cdot A_m}{\pi\cdot NEP\cdot SNR_T}} \tag{8}$$

For the case of an unresolved target, we can write y_2=2×Lambertw(x_2) where $y_2=\sigma R$ and

$$x_2=\sigma/2\cdot\sqrt[4]{S_2}=\sigma/2\cdot\sqrt[4]{\frac{\eta\cdot P_L\cdot G\cdot A_m\cdot A_T\cdot 4}{NEP\cdot SNR_T\cdot\pi\theta^2}} \tag{9}$$

We see that the range equations are easily transferred to the Lambert's W function. This function is depicted in Figure 1. By studying this function and its derivative, we can have a better understanding on how range is dependent on the overall system, target, and atmospheric (underwater) parameters. A more detailed discussion on the use of the LambertW function in ladar performance calculation is found in Ref. [10].

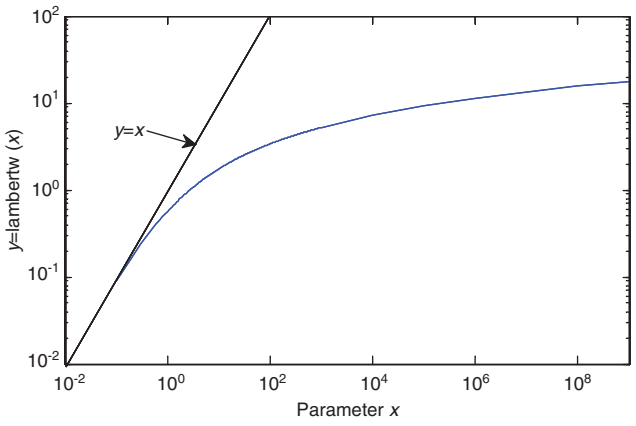

Figure 1 The function y=Lambertw(x) calculated in MATLB©.

An interesting example of the use of the Lambert solution might be to consider different detector arrays of size N*N pixels. For the resolved target, this means that the available laser power per pixel is divided by $1/N^2$, and the parameter x is reduced by $1/N$ for a fixed pulse energy. In this way, the influence on the maximum range for different array sizes and fixed laser emissions may be studied. The corresponding reduction in x for a small target detected by an array at a fixed laser power is $1/N^{1/2}$.

2.1 A system example

We will illustrate the use of the equations above by looking at two kinds of short-pulse active imaging systems. Let us consider two types of systems having the same average power using either flood illumination or scanning. The parameters are given in Table 1.

Figure 2 illustrates how the maximum range (for SNR=7) varies vs. visibility against an unresolved target and parameters according to Table 1. The variations are directly related to the general Figure 1. For increasing visibilities, the maximum range increases to a saturation level set by the system margin. This margin depends on

Table 1 Perimeters used for the two active imaging systems.

Parameter	Notation	Flood illumination	Scanning
Laser average power	P_{av}	1 W	1 W
Laser prf	f_p	20 Hz	10 kHz
Laser pulse time (FWHM)	τ	5 ns	5 ns
Laser peak power $=P_{av}/(\text{prf}\times\tau)$	P_L	10^7 W	$2*10^4$ W
Laser wavelength	λ	1.57 µm	1.57 µm
Receiver area	A_r	$\pi x(0.15)^2/4$ m^2	$\pi x(0.15)^2/4$ m^2
Nr of illuminated detectors		N×N	N=1
Focal length	F	1 m	1 m
Receiver optical loss	T_{opt}	0.7	0.7
Optical filter	$\Delta\lambda$	30 nm	30 nm
Total system efficiency	η	0.25	0.25
Detector size	a_d	24 µm (pixel)	200 µm
Detector FOV	$IFOV$	24 µrad	200 µrad
Detector dark noise current	$\overline{I_{DN}^2}$	-	3.5×10^{10} A
Preamplifier noise current	$\overline{I_{PN}^2}$	-	10^{-8} A
Background noise current	$\overline{I_{BN}^2}$	-	$5.3*10^{-11}$ A @B=300 MHz
Photo-detector gain	M	-	10
Excess noise factor	F	-	5.5
Unity-gain responsivity	R_D	-	0.93 A/W
Noise equivalent power sun	NEP	(1.33 pW) 0.1 nW* * assumed more realistic and used in the example	3.33 nW
Noise equivalent power night	NEP	(1.33 pW) 0.1 nW*	3.31 nW
Target reflectivity	ρ	0.15	0.15
Background reflectivity	ρ_{bcgr}	0.05	0.05
$\text{SNR}_{\text{treshold}}$	SNR_T	7	7
Viability	V	0.5–30 km	0.5–30 km
Ext. coefficient	$\sigma=0.31(3/V)^{1.11}$	2.26–0.024/km	2.26–0.024 /km
Backgound spectral irradiance	E_λ	0–170 W/m^2 µm	0–170 W/m^2 µm

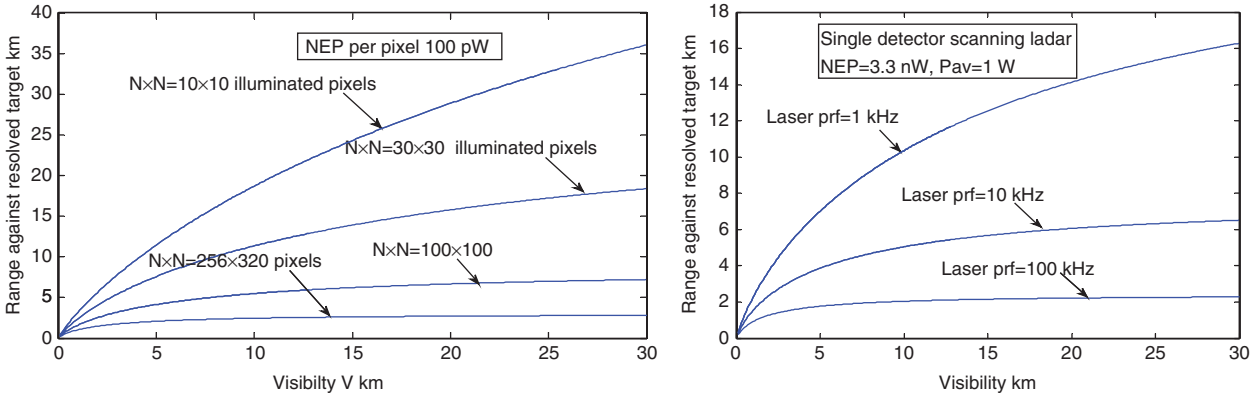

Figure 2 (Left) Maximum range (for a signal-to-noise ratio threshold, SNR=7) for a gated imager looking against a resolved target vs. visibility with the number of illuminated pixels N×N as a parameter. Average power 1 W and prf=20 Hz. (Right) The corresponding for a scanning single pixel system also with 1-W average power and much higher and different laser pulse repetition frequencies (prfs).

the parameter x defines above. For an active imager, there is, for example, a max range penalty in increasing the number of illuminated pixels, for example, as illustrated in Figure 2. For a scanning single pixel, there is a similar balance between the maximum range and the total search time [given by the pulse repetition frequency (prf)] as seen in Figure 2, right part.

3 Ex. of active imaging systems

3.1 Continuous wave (CW) illumination systems

Active imaging can be made with CW, modulated or pulsed laser sources. Active imaging using CW lasers has the advantage of simplicity as it can be realized with simple and less costly cameras and sources. Combining image intensifiers in the near infrared (NIR; 0.7–0.9 μm) and low-light TV or short wavelength infrared (SWIR; 1–3 μm) cameras with a simple laser diode illuminator gives a compact system, which combined with thermal cameras gives a system for both for search and identification (See Figure 3).

Examples of laser illumination systems include mine detection systems [11, 12] and surveillance and targeting systems and many others [13]. Broadband illumination using laser diodes, for example, will also reduce target-induced speckle noise of the image. Imaging at even longer wavelengths in the 3- to 5-μm region has the advantage of having a lower influence of turbulence and better haze penetration than shorter wavelengths. Recent development in laser diodes can produce handheld eye-safe lasers with output powers in the W regime at 1.5 μm

Figure 3 (Left) The camera (OWL SW1.7 CL 640) from Raptor Electronics including a telescope lens and a 1.5-μm, 1.6-W laser illuminator on the top. Images on the upper and lower rows show the passive (day time) and active images (during night), respectively. Range to the text board was 400 m and to the control tower, 2.5 km. Images FOI.

[14] and in the MWIR as well as in the longwave IR (LWIR) band [15]. Illumination systems using laser diodes have the potential of reducing target-induced speckle noise [16].

3.2 Range-gated systems using flood illumination

By using a camera with time-gated functionality, we obtain several advantages compared with the simple illumination system discussed above. The gating gives a possibility to extract the target from the background, see through obscurants, and also reduce the effect of the optical background light during the short gate. By sweeping the gate over the target, it is possible to achieve 3-D images with much higher range resolution than that given by the laser and gate length [17].

Placing the gate behind the target enables the target to be seen in silhouette, which often can be of great value in defense and security applications, for example, to reveal weapons sticking out from a body [18]. Figure 4 shows the advantage of combining a thermal imager for target detection with a pulse-gated system for target recognition. Gated systems based on low-prf high-pulse energy are often motivated by using the existing laser range finder/laser designator also for imaging. Examples of military applications of range gated imaging that are close to operational use are pod-mounted systems (the US LTIP) and ground systems for long-range ID (the US LRID). DARPA has a program called SPI-3D Standoff Precision ID in 3-D (SPI-3D) [19]. Instead of gain coding during the pulse, the switching of polarization is made so that range information can be obtained from a single pulse. In Europe, both Selex in the UK and Thales have been developing 1.5-μm gated imagers. These involve the Technology Demonstration Program Joanna, a demonstrator of a multifunction optronic pod. Thales has developed Damia, a 1.5-μm pre-operational laser imaging solution that was integrated into their Damocles [20]. Selex is developing an interesting system called PicoStar [21], which combines SAR with an EO subsystem, implementing the latest dual-mode imaging sensor together with a conventional zoom/e-zoom TV sensor. The 640×512 pixel Swan II sensor provides conventional passive MWIR imaging at 3–5 μm together with active-gated imaging at 1.57 μm. Laser designation, rangefinding, and target illumination is provided by the same laser.

Instead of using a pulsed laser rangefinder or designator for imaging, several companies and research organizations are using high-prf diode lasers for range-gated imaging. Obzerv [22] in Canada manufactures range-gated systems based on the laser diode DALIS™ illuminators at 860 nm. This high-rep rate and short wavelength gives very clear speckle-free images enabling car license plate reading above 1.2 km using a 24-cm aperture with a magnification between 60 and 240 times. Elbit [23] in Israel manufactures systems with similarities with the Obzerv systems, by using laser diode illuminators.

Recently, other modulation techniques have been studied, for example, a linear gain variation within the gate to extract range and intensity information. This can be done by taking the ratio between images taken with linear and constant gain. The advantage with this method is that the results is independent of the shape of the laser pulse and that 3-D imaging can be obtained with 1–2 pulses instead of about 5–10. The method has been experimentally verified [24]. Laurenzis et al. [25] have developed a 'super resolution technique' by combining two images from a trapezoidal convolved gate/laser pulse to obtain high range resolution. The strict linear dependency of the rising slope was used to develop a simple model for the reconstruction of the depth information. Laurenzis [26] also develops an elegant method based on comparing range-delayed signals using a Lissajous-type

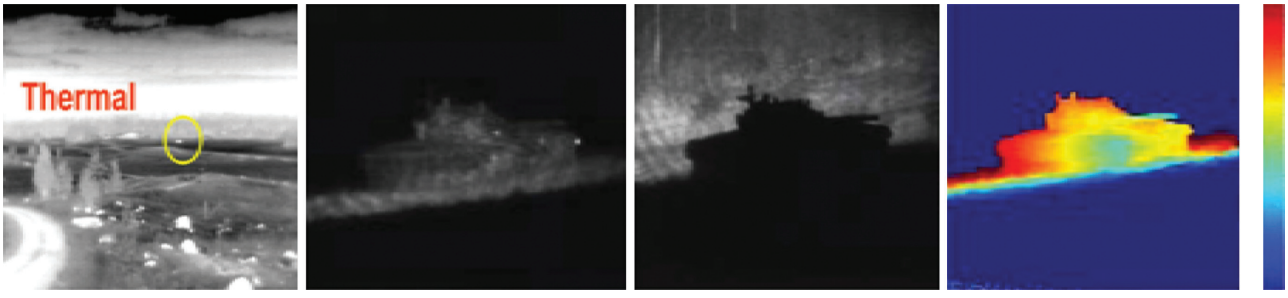

Figure 4 (Left) A potential target detected by a thermal imager. The next images show the target being observed by the range-gated laser system in the illumination, silhouette, and 3-D reconstruction mode. The range resolution is in the order of 20 cm despite the much lingered gate and pulse length. Images FOI, see Ref. [13].

eye pattern to define clear criteria for depth resolution and depth mapping capabilities of an active imaging system.

APD arrays based on CMT are being developed for active gated imaging in the SWIR region by several actors like Sofradir/Leti [27] and Selex [28], for example. Detectors based on InGaAs [29–31] and InGaAs/InP TE EBCMOS [32] have also been reported.

3.3 Full 3-D imaging systems

Range-gated imaging or active 2-D or 2.5-D, as it is sometimes denoted, has its drawback in 'gate' management. A full 3-D sensor referring to a 3-D/intensity image using one laser pulse has many advantages and will, in the long perspective, replace range-gated systems. Note that the range-gated function is a functionality, which easily can be implemented in a 3-D imager.

A full 3-D imager will more rapidly facilitate such functions as detection of hidden targets, automatic or aided target recognition, mapping, and threat detection. 3-D imaging has so far, to a large extent, been made by scanning laser radars, but 3-D arrays have during the last years come into use. The prime military application for 3-D imaging, at least from an investment point of view, has so far probably been weapon guidance.

The JIGSAW system was a DARPA-initiated development aimed for a small UAV to detect and recognize target under trees. This is done by stiching together a number of 3-D point clouds taken from different views [33, 34]. The whole system, including a 12-inch gimbal, weighs 45 kg. Figure 5 illustrates the power of 3-D imaging ladars to see through vegetation by 'range cropping'. The basic presumption is that enough pixels are seen thight the vegetation cover and hitting the target either in a single look dense sampling (left image in Figure 5 or by fusing multiple looks (next two images in Figure 5). Special filter techniques have been developed to detect and classify vehicles under occlusion [35].

Photon counting in the Geiger mode domain has been used in lidars and the US JIGSAW program. Detector arrays based on photon counting are now commercially available from Princeton Lightwave [37] and Boeing Spectrolab and others up to fomats of 32×128 and with 128×128 in development. Raytheon is developing linear-mode photon-counting arrays in sizes up to 256×256 elements. Linear-mode photon-counting arrays provide significant advantages when compared to Geiger-mode counting arrays developed by MIT and others. These advantages include absence of after pulsing and dead time, nanosecond pulse-to-pulse temporal resolution, and robust operation in the presence of high-density obscurants or variable reflectivity objects [38]. Raytheon claims that dark current rates as low as 1/s can be achieved. Sofradir/Leti [27] and Selex [28] have both developed 3-D sensing arrays based on CMT inf the half TV format (320×256 pixels).

3.4 Aerial mapping systems

Airborne and vehicle-borne laser mapping using scanning lidars has been a success especially for civilian applications. A recent book which gives a good overview on topographic laser scanning has been published by Shan and Toth [39]. Lidar mapping is now beginning to enter military operations. The use of laser mapping will generate high-resolution range and intensity synthetic environments, which can be used for mission planning and battle damage assessment but also as a reconnaissance tool utilizing the 'see through' or change detection associated with high-resolution 3-D data.

Recent trends have been to make the systems small and compact as well as combining laser scanning with digital and hyperspectral cameras. One example of a compact system is shown in Figure 6. This system,

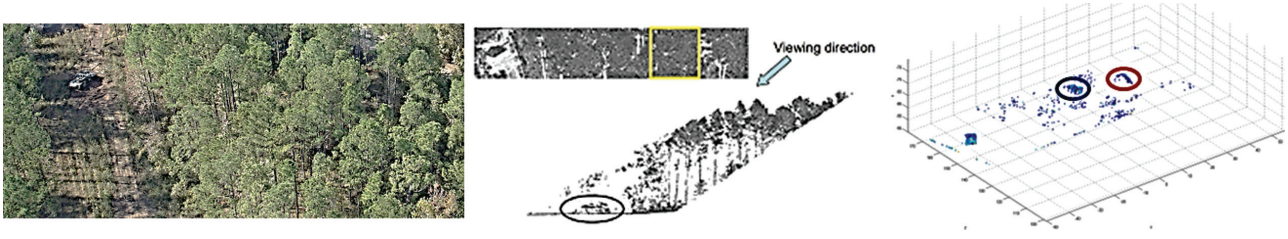

Figure 5 (Left) A part of vegetation with three vehicles, two of them occluded. The middle image shows an example of the power of 3-D ladars to see through vegetation. Above is the intensity image, and below is the 3-D image of the area within the square. The target (a tank) is encircled. The next shows all three vehicles visible (the occluded are encircled) and suitable for classification, for example, by template matching. Images FOI [35, 36].

developed by AHAB in Sweden, is called HawkEye III and is a combined airborne bathymetric and topographic multisensor lidar system, containing:

- A 10-kHz bathymetric channel optimized for high accuracy and high data density surveys in deep water to kD=4. D is the depth, and k is the diffuse attenuation coefficient in the water.
- A 35-kHz bathymetric channel, optimized shallow water region up to depth kD=2 through the transition zone and up on land.
- A 400-kHz topographic channel that provides the detail and resolution in the data that even your most demanding topographic lidar application requires.

The HawkEye III captures the full waveform in all channels, deep bathy, shallow bathy, and topographic. Other well-known lidar providers include Optech, Leica, Riegl, and others.

NASA has been in the forefront in developing airborne lidars. The Airborne Oceanographic Lidar (AOL) was sponsored jointly by NASA and NOAA. AOL was continually modified and upgraded over a 20-year period. Both topographic and bathymetric applications were studied. The NASA EAARL lidar [40] is a raster-scanning, temporal waveform-resolving adaptive lidar, which also contains a down-looking color (RGB) camera, and a high-resolution color-infrared (CIR) digital camera. NASA had a program called Vertical Canopy Lidar (VCL) for motoring canopy heights from satellite. An airborne lidar built for verification of VCL is called Laser Vegetation Imaging Sensor (LVIS) [41]. In Europe, laser mapping for forestry has been a subject of research for more than two decades. Important contributions have been made for forestry by the Scandinavian countries and Canada. A summary of the methods used for forest inventory can be also be read in the paper by Hyyppä et al. [42].

Military-driven terrain mapping will focus on capabilities like reduced vulnerability, covertness, high area coverage rate, and high spatial resolution even from high altitudes. The present lidar technology is focused on analog detection of pulses in the 10- to 100-μJ range and relatively large optics to obtain return signals of thousands of photons per shot. This technique has its limitations due to the fact that the laser pulses cannot be too short and still have high energy pulse energy without jeopardizing eye safety and optics damage. The SNR has to be rather high to get the range accuracy down to the cm level. An alternative could be to use photon-counting techniques to allow the range to be obtained from even a single photon return.

The potential advantage of photon-counting lidars includes reductions in the size, weight, and power. On the other hand, the range accuracy can be high in the photon-counting mode, and the low demand on laser power will allow high spatial resolution even from high altitudes. The US Air Force ALIRT system uses a Geiger mode array receiver, and this system has recently been used in the analysis of the earthquake in Haiti [43]. Recently, the head of DARPA cited the high-altitude Lidar operations (HALO) lidar project as an example of DARPA's commitment to rapidly serve the troops. HALO allows collection of high-resolution 3-D data, down to fewer than 10 photons and is 10 times faster than state-of-the-art systems and 100 times faster than conventional systems [44].

The company Sigma Space Corporation [45, 46] has demonstrated a multibeam photon-counting lidar capable of recording 2.2 megapixels per second, with a spatial resolution of 15 cm, and vertical resolution of 3 cm from 1000-m altitudes. The systems uses a Nd:YAG microchip laser producing few microjoule subnanosecond pulses at fire rates of up to 22 KHz. The beam is broken into 100 separate beams and detected by a 10×10 PMT array from

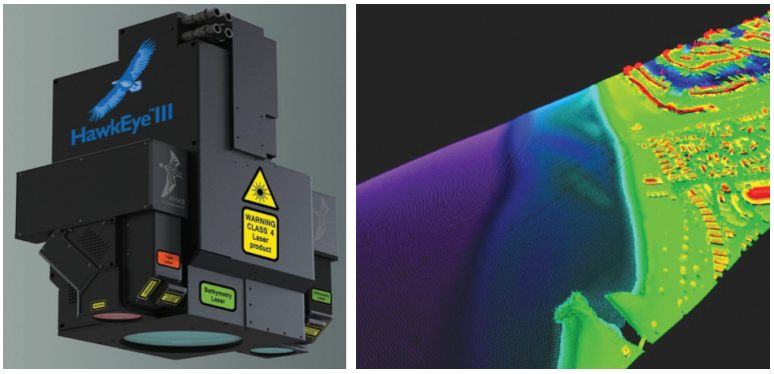

Figure 6 Example of a state-of-the-art airborne mapping lidar, the Swedish HawkeEye III developed for delivering a seamless map of both bottom and land topography. Image AHAB Sweden (http://www.airbornehydrography.com/content/hawkeye-iii).

Hammamatsu. The detected photon pulses are timed and stored using a company proprietary 100-channel parallel timing unit with 100-ps resolution. With a volume of 2 cubic feet and 25 kg mass, the system lends itself to use on UAV:s.

3.5 Terrestrial laser scanners

Laser scanners have been used on unmanned ground vehicles for navigation and obstacle avoidance. The most widespread demonstration on the success of laser scanners in UGV:s has probably been the DARPA grand and urban challenges [47] where laser scanners were the key sensors. The Lynx system from Optech Inc. is one example of many commercial road mapping laser systems [39].

4 Adding the spectral dimension to laser imaging and mapping

Current laser imaging and mapping systems are mostly based on single, fixed-frequency lasers, generally in the near infrared and often in the so-called eye-safe region SWIR region (1.5 μm). On the other hand, great progress has recently occurred in passive multi- and hyperspectral imaging with applications ranging from environmental monitoring and geology to mapping, military surveillance, and reconnaissance. Data bases on spectral signatures allow the possibility to discriminate between different materials in the scene. Present multi- and hyperspectral sensors generally operate in the visible and short wavelength region (0.4–2.5 μm) and rely on the solar radiation. The measured radiance in the sensor is, however, difficult to relate to spectral reflectance units due to the dependence on a number of external sources and phenomena such as, e.g., solar angle, clouds, shadows, atmospheric scattering, or extinction. These variations increase the uncertainty to derive reflectance spectra and to relate these to data bases for material identification.

4.1 Imaging

An active spectral imaging will largely overcome these difficulties by offering a complete control of the illumination. In addition, it will bring all the advantages already sought when using single-frequency active imaging: night and low-light operation, penetration, access to polarization information and to high-resolution 3-D information. Hence, fusing the knowledge of range-resolved ladar and passive or active spectral imaging will result in new capabilities in the field of EO sensing. An overview of active imaging with focus on spectral imaging was recently made for the European Defence Agency (EDA) [48, 49]. New capabilities in spectral imaging including active imaging are also discussed by Lewis [50].

Most of the work, so far, in active spectral imaging for military and security seems to be limited to laboratory investigations. Broad spectral emission will reduce the speckle noise in active imagery [51], for example. A group at MIT has been exploring active spectral sensing in more detail [52]. They conducted a series of laboratory and field tests to demonstrate the utility of combining active illumination with hyperspectral imaging for the detection of concealed targets in natural terrain. The system was deployed under a variety of environmental conditions, including nighttime illumination, and on a variety of target scenes, including exposed and concealed plastic and metallic mine-like targets. Targets have been detected and identified on the basis of spectral reflectance, fluorescence signatures, degree of polarization, and range-to-target information (via range gating). The MIT group discovered that water vapor absorption lines in the SWIR are exploitable sources of contrast that enable us to distinguish between natural and man-made objects. Man-made objects, for example, paints and plastics, repel water, while vegetation and soil absorb water. As water is highly absorbing at 1.4–1.5 μm but not so much at 1.6 μm, a simple intensity ratio between images at these two wavelengths will enable to distinguish between man-made and natural objects.

Active hyperspectral imaging has also been investigated by BAE in the UK [53, 54]. The project at BAE was sponsored by the EMRS DTC and involved both simulation and laboratory demonstrations. A comparison between the best active systems with a generic passive, multispectral LWIR sensor was made showing the advantage of the active system due to increased noise for the LWIR system.

Thales and CNRS in France in collaboration with Norsk Elektro Optikk (Norway) report on the design and exploitation of a real-field laboratory demonstrator [55]. It was found that good detection performances rely on the joint use of intensity and polarimetric images, with these images exhibiting complementary signatures in most cases.

An interesting range imaging spectrometer has been presented by Kinder et al. [56]. The spectrometer can simultaneously obtain 3-D spatial and hyperspectral data. The ranging-imaging spectrometer (RIS) is based on the computed tomographic imaging spectrometer (CTIS)

developed at the Optical Science Center, and the scanner-less laser radar (Ladar) architecture developed at Sandia National Labs.

A recent interesting experiment using a multispectral mid-infrared laser stand-off imager was reported by Wang et al. [57]. The system was applied to diverse targets that consisted of man-made and natural materials and objects, and showed capability to resolve and distinguish small spectral differences among the various targets. Colorless objects in the visible were shown with 'colorful' signatures in the mid-IR. The system design was according to the authors suitable for compact packages with semiconductor lasers, and the results suggest that laser-based multispectral imaging can be a unique and powerful technology for target discrimination. Figure 7 illustrates how different materials, which seem rather similar in the visible, can be differentiated by active mid-IR imaging.

Hardie et al. [58] has also investigated the potential of mid-IR imaging ladars.

Simard et al. [59] have investigated hyperspectral imaging using a range-gated camera by observing fluorescence spectra from mines and vegetation. For the surface mine detection application in mind, the preliminary result indicated that the false alarm rate associated with this scenario of detecting surface-laid mines might be too high for a ground area scanning speed of practical interest. A Danish group has also demonstrated multispectral high-resolution 3-D imaging [60]. By exploiting Raman scattering in single-mode optical fibers, multispectral light was generated from a green nanolaser with a high pulse repetition rate. Each pulse triggered a picosecond camera and measured the distance by time of flight. Three-dimensional images were then constructed with submillimeter accuracy for all visible colors.

Powers et al. [61, 62] present a ladar for UGV applications for a combined ATR function using a combination of spectral and spatial imaging. The results are discussed here in the context of autonomous vehicle navigation and target recognition. The laser emitted nanosecond super-continuum pulses generated in a photonic crystal fiber. Each of 25 spectral bands was independently range resolved with multiple return pulse recognition. Cathcart et al. [63] discusses EO signatures for personnel detection in urban environments. They point to the importance of the SWIR region especially for nighttime classification of people.

Stothard et al. [64] demonstrated a system for the active real-time hyperspectral imaging of gases using a continuous wave, pump-enhanced, optical parametric oscillator and an electromechanical polygonal imager (Figure 8). This technology has also been applied to liquids [65]. The wide spectral coverage and high spectral resolution characteristics of this source allowed the system to be selectively tuned into the absorption features of a wide variety of species. Recently, the technique has been extended to cover hazardous materials [66] including unknown chemical warfare agents [67]. A transfer to LWIR region, between 5 μm and 12 μm will increase the identify-cation capability due to more characteristic fingerprints in this wavelength region.

One area in which spectral imaging has been studied to a great extent is the area of stand-off detection of explosives. The methods of laser spectroscopy are most promising for fast stand-off detection and identification of traces of both known and new types of explosives in multicomponent media [68]. Spectral imaging is ideal for localizing and verifying small amounts of explosives (the amount of explosives in a fingerprint on object surfaces is ~10 μg) because the pixilation enables the background to be suppressed. Figure 9 illustrates an imaging stand-off laser system based in Raman detection and an ICCD receiver. By centering the liquid filter on the different material-specific Raman peaks, images of the occurrence of the different substances can be obtained [69, 70].

Besides Raman, other spectroscopic techniques have been used in active spectral imaging for stand-off explosive

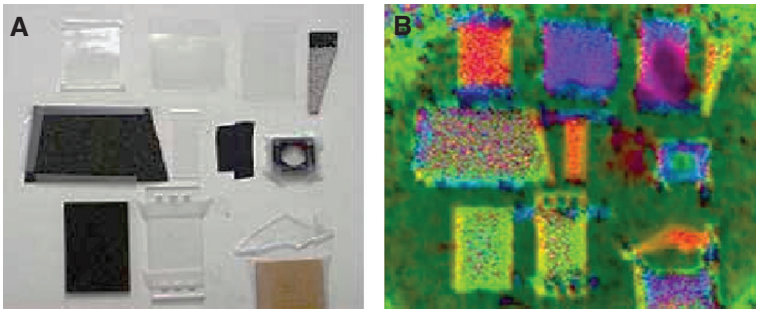

Figure 7 (A) Images in visible light; (B) differentiation based on material reflectivity in mid-IR. From Wang et al. [57].

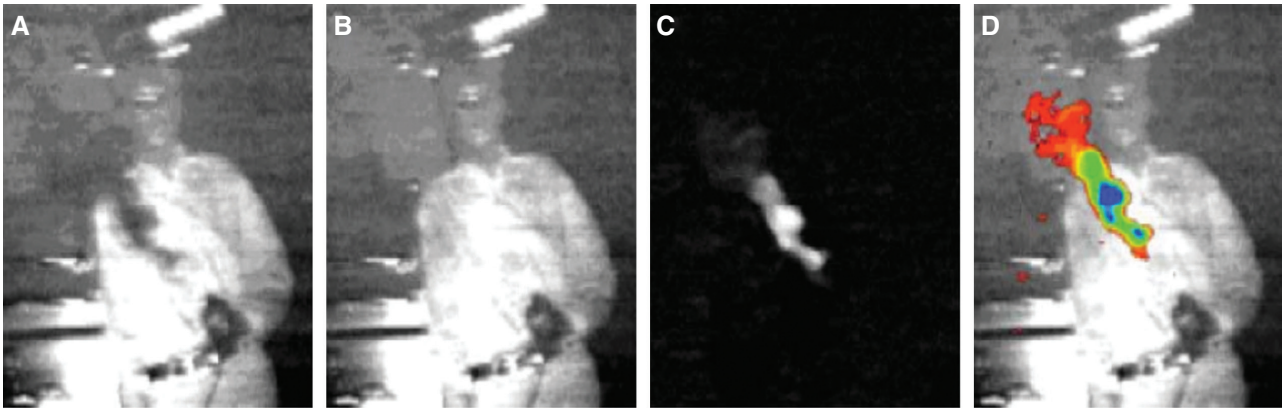

Figure 8 Image enhancement using the differential absorption. (A) and (B) show images captured ON and OFF methane absorption lines. The difference between these images (i.e., the methane plume) is shown in (C). Finally, false color is applied to (C), which is then superimposed upon (B) to generate (D). From Stothard et al. [64].

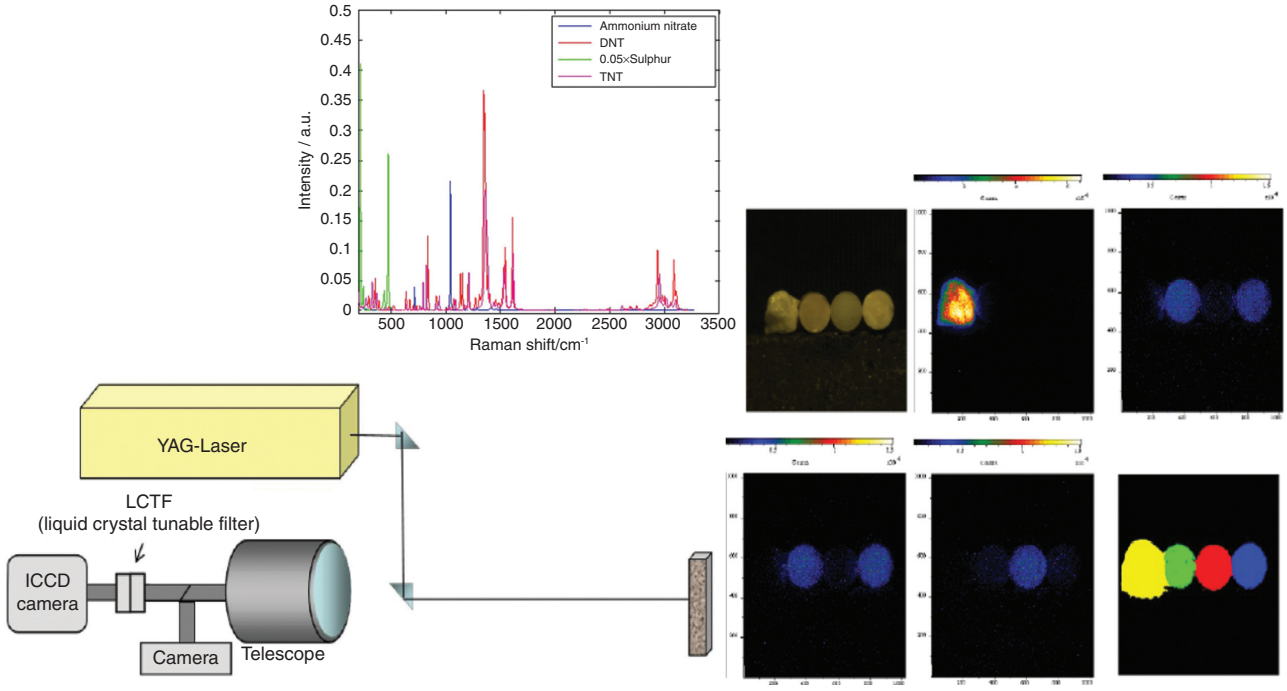

Figure 9 (Left) Experimental setup for the imaging Raman experiments. Distance between setup and sample was 10 m. (Right) From top left to bottom right, in order: white light image of the four samples sulfur, DNT, AN, and TNT (in order as occurring), intensity image at 473 cm^{-1} corresponding to sulfur peak, intensity image at 1347 cm^{-1} corresponding to DNT peak, intensity image at 1043 cm^{-1} corresponding to AN peak, intensity image at 1358 cm^{-1} corresponding to TNT peak, false color coding image where yellow represents sulfur, green DNT, red AN, and blue TNT. Images from FOI [69, 70].

detection like IR photothermal imaging and hyperspectral imaging in scattered light (see [71] for an overview).

Besides the more well-known methods for remote sensing of chemical substances including explosives, such as Raman techniques, fluorescence, and laser-induced breakdown spectroscopy (LIBS), the infrared reflection/absorption spectroscopy is seen as an interesting option. This is, in part, linked to the development of the quantum cascade laser (QCL), which is a semiconductor diode laser with tunable emission in large parts of the IR spectrum.

Goyal et al. [72] have investigated the LWIR reflectance of contaminated surfaces using a quantum-cascade laser (QCL), which are reconciled between 9.1–9.8 μm and a HgCdTe array detector (FPA). A liquid chemical was applied to a variety of substrates that diffuse reflective gold, concrete, asphalt, and sand. Experimentally measured

signatures were found to be in accordance with theoretical calculations. Clear signatures were also obtained for contaminated concrete, asphalt, and sand. These measurements demonstrate the potential of this technique to detect and classify chemicals on outdoor surfaces.

Bauer et al. [73] present methods for detection based on photofragmentation and subsequent mid-IR detection for sensing nitrogen-based explosives. Furstenberg et al. present similar techniques [74].

A group from Fraunhofer Institute has presented a number of stand-off imaging results in explosive detection [75, 76]. They demonstrate contactless detection of solid residues of explosives using mid-infrared laser spectroscopy. The method is based on active laser illumination, synchronized with the collection of the backscattered radiation by an infrared camera. The key component of the system is an external cavity quantum cascade laser with a tuning range of 300 cm^{-1} centered at 1220 cm^{-1}. Residues of trinitrotoluene (TNT), pentaerythritol tetranitrate (PETN), and cyclotrimethylenetrinitramine (RDX) could be identified and discriminated against nonhazardous materials by scanning the illumination wavelength over several of the characteristic absorption features of the explosives.

There are clear advantages of IR spectroscopy for stand-off remote sensing in that it is possible to make eye-safe systems even for long-range detection. Moreover, due to the availability of compact lasers with high power and possibility of tuning the wavelength over a relatively broad frequency range, the prospects of compact and robust commercial systems are good.

Before detecting and verifying explosives, a robust method for localizing mines and IEDs is needed. The detection of mines and IEDs are a formidable problem for defense forces around the globe. A manifold of active and passive spectral methods have been tried. At FOI, we have investigated both passive and active spectral imaging in combination with high-range resolution for surface mine detection [77]. The high-range resolution is of special value in a detection mode where new objects can be detected by observing the distance change in a point cloud. This type of detection can also be applied to passive sensing [78]. Figure 10 shows an example of active spectral imaging of mines and mine-like objects on grass as detected by white light illumination in darkness. Powerful white light lasers can replace conventional lamps for this application.

One interesting problem for defense and security is to investigate to what degree one can 'see colors' at night, that is, using, for example, NIR and SIWR illumination. In that case one could distinguish between individuals due to their clothing, for example, which usually is hard by using

Figure 10 An example of multispectral imaging with white light illumination using a flashlight. Note that the spectral bands of the sensor were not optimized for the purpose, and further improvement can therefore be expected. (Left) Photo. (Middle) The image shows the PCA components 3, 2, and 1 as RGB of the original image. Detection using the PCA component 3 is exhibiting very low false alarm rate (right). Image FOI from [77].

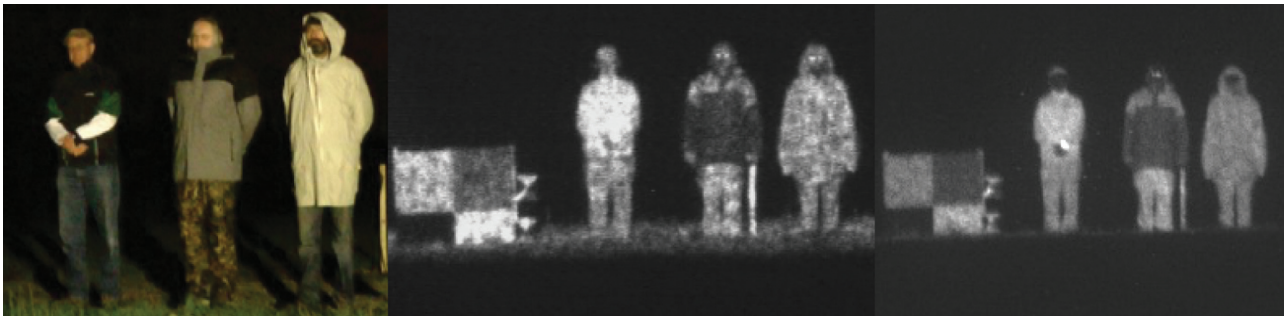

Figure 11 Clothes measured from 800 m distance. (Left) visual, (middle) active NIR image, (right) active 1.5 μm. Clothes from left to right in each image: jogging dress, jeans, and beige cap. 2: Gray jacket and Swedish hunting pants (A). 3: White anorak (item G), jeans (item H), and black cap. Note the shift of contrast between the different garments for the visual vs. NIR and SWIR region. Images FOI from [79].

thermal IR. Another capability is to increase the detection of people against urban and vegetation backgrounds. This has been investigated in multinational measurement campaign in France [79]. Figure 11 shows some clothing imaged in the visible and active NIR (808 nm) and SWIR (1550 nm) regions. It is clear the contrast between the different garments is changed rather drastically when moving from visible to the NIR/SWIR regions. The chosen wavelength was not optimal for cloth separation as can be seen when investigating the spectral reflectance [79].

We also observe that some speckle patterns seem to be more dominant for the active 808-nm system compared with the 1550-nm system, which is probably due to the increased turbulent scintillation for the shorter wavelength in the NIR region.

The reflectance of the clothes in the NIR/SWIR regions will also often be higher than that found in typical urban materials, such as concrete. Figure 12 illustrates the contrast of a person seen against grass and bushes. This contrast seems more pronounced at 1550 mn than at 808 nm.

Farley et al. investigated the soldier's camouflage equipment using multispectral and hyperspectral sensing [80], and Zhou et al. [81] describes camouflaged target detection based on visible and near-infrared polarimetric imagery fusion. Hogervorst et al. [82] evaluates urban camouflage using human observers.

The combination of photon-counting arrays and supercontinuum lasers shows promise for both military and civilian remote sensing [83]. One complexity is the spectral discrimination in the receiver. Goda et al. [84] recently demonstrated a new active hyperspectral concept transforming a 2-D image into a time dispersed signal, which was captured by a single detector. This method should, in principle, be applicable to an array of optical fibers, each for one pixel and having its own dispersive fiber separating different wavelengths into the time domain. This could also be used to transform a fixed wavelength 2-D intensity image to a single detector by using different time delays in different fiber channels and this marking each pixel.

4.2 Mapping

Multispectral lidar systems provide unique new opportunities for remote sensing of mainly topography but are also of interest for hydrography. The laser emits multiple wavelengths simultaneously and can combine high-resolution vertical information with spectral information in the form of, for example, the photochemical reflectance (PRI) and normalized difference vegetation index (NDVI), which measures the amount of living vegetation. Compared to the conventional way of combining a passive multi or hyperspectral sensors with lidar, a multiwavelength lidar gives advantages such as:

- Generation of reflection data independent of sunlight
- Penetration of otherwise shaded areas where a passive sensor has difficulty
- Providing the ability to separate the tree and bush vegetation from other ground vegetation

Figure 12 Person in a dark green uniform against bushes and a concrete wall, range 800 m. (Top left) visual, (top right) passive 808-nm image. (Bottom left) visual, right: 1550 nm active imaging using a 30-m gate. From [79].

The ability to perform such measurements will allow better mapping of the forest structure and the processes that are directly related to photosynthesis. It will, therefore, significantly improve our ability to measure and map the terrestrial biosphere and understanding of the carbon cycle, the land use, and biodiversity.

So far, mainly laboratory measurements and theoretical modeling have been published on multispectral lidars. One concept that is studied is the multispectral canopy lidar (MSCL) [85, 86]. In this concept, four laser wavelengths (531/550 nm and 690/780 nm) are used to collect the PRI and NDVI data. Design studies for the use of this type of lidar from space is underway in Europe [87].

Hakala et al. [88] presents the design of a complete waveform lidar based on a continuum laser with tunability from the visual to the NIR/SWIR (480–2200 nm) range. The lidar generates 3-D point clouds using spectral reflectance data backscattered from which a variety of parameters on vegetation condition can be derived from chlorophyll content, water content, and PTRI and NDVI index. Figure 13 provides an example.

In midrange, 3-D terrain mapping, the operational needs for airborne military reconnaissance include detecting and identifying military vehicles in a rural environment, and mapping and classifying urban areas. Increased performance would be obtained by using multispectral active imaging. A combination of three wavelengths in the SWIR should be appropriate, with a relative freedom in the choice of wavelengths [49].

Lidar in hydrographic applications multispectral lasers, preferably in the visible wavelength region where the water transmission is reasonably high, provides new opportunities to determine the water inherent optical properties [89] as well as better opportunities for bottom classification [90, 91]. One example of a multispectral imaging capability to distinguish certain types of algae from each other is shown in Figure 14. The small amounts of ceramium, hardly visible in the photo, are clearly detected with the characteristic red algae fluorescence in the 580-nm and 650-nm bands, where other species have low fluorescence emission. The fluorescence emission from chlorophyll at 680 nm is high for the 1-year old fucus plant, slightly lower for the 4-year fucus plant, and relatively low for cladophora. See also [91] for the spectral fluorescence signatures from species measured with excitation source at 532 nm.

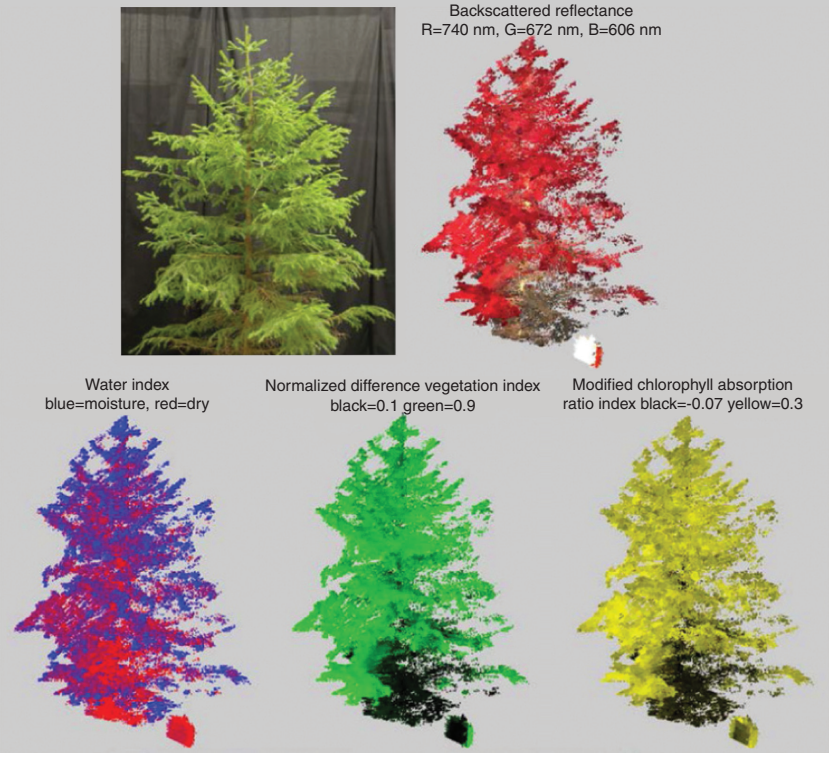

Figure 13 A photograph of spruce and associated 3-D point cloud displays various data products derived from the backscattered response of a laboratory measurement with a multifunction lidar. To reduce the noise in the spectra, an average of 5-cm voxels was used. The spectral indices were calculated for each voxel, and the results are shown in full 3-D point cloud colors for different indices related to the tree condition. From Hakala et al. [88].

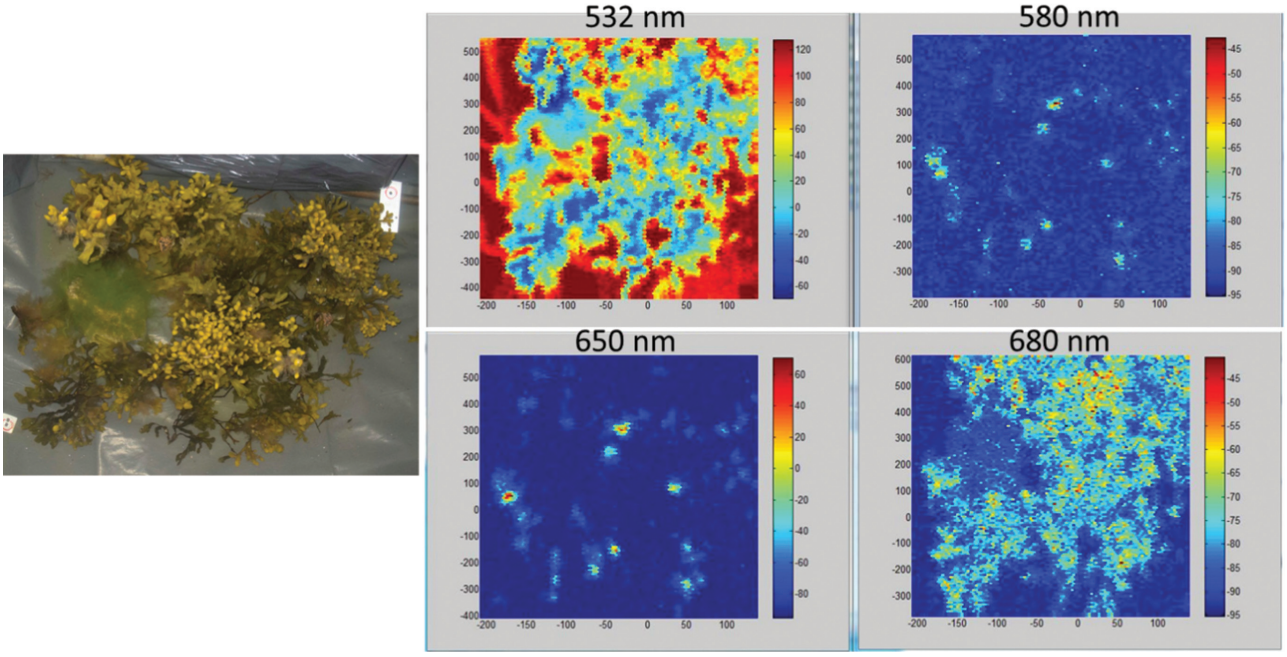

Figure 14 (Left photo) A mix of bright 4-year old and 1-year (brighter) bladder wrack (*Fucus vesiculosus*), the green algae *Cladophora* , and small amounts of the red algae *Ceramium*. Right four fluorescence images induced by 532-nm laser excitation. The image 532 nm is the elastic image, and the 580 nm, 650 nm, and 680 nm show the fluorescence images within 10-nm bandwidth of the center wavelength when the samples were scanned with the 532 nm laser. Images FOI.

A fusion of passive hyperspectral data with 3-D data from a lidar enables estimation of shadow regions from which a classifier can learn about how the spectral signature behaves in shadows [92, 93, 94]. A method is suggested to correct spectral signatures from estimated light conditions at a certain geographical position, and the combination of spectral and spatial information from the lidar is used to find objects in shadowed areas. An example of shadow detection is illustrated in Figure 15.

The Coastal Zone Mapping and Imaging Lidar (CZMIL) is an example of a new advanced lidar system for coastal mapping in US waters [95]. The system combines laser with a hyperspectral camera, and a digital camera can produce simultaneous high-resolution 3-D data and images of beach and seabed in shallow waters. Advanced products include coastal topography, benthic classification, and characterization of water quality in both clear and turbid waters.

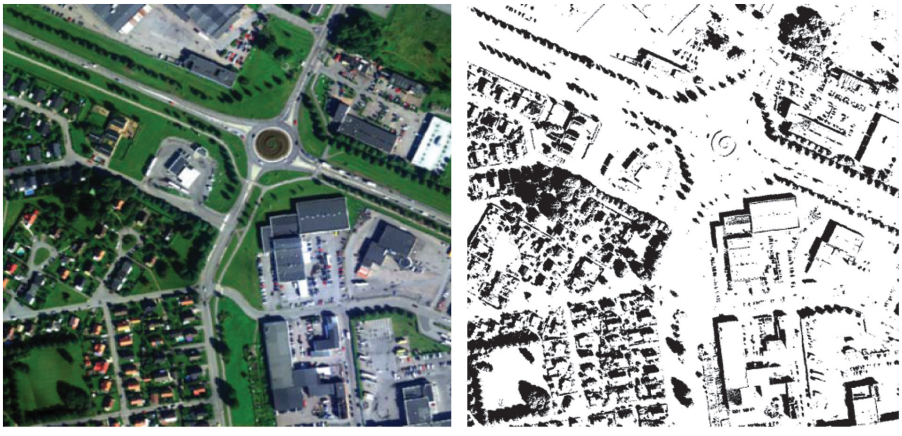

Figure 15 (Left) An image for a hyperspectral sensor showing three bands (corresponding to RGB) of a total of 24 bands. Right automatic detection of shadows with the help of 3-D lidar data. Images FOI.

5 Signal processing for active spectral imaging and mapping

A full utilization of the richness of target features that ladars provide needs advanced signal processing techniques and methods. Examples of such features, which can be extracted and used for discrimination, have been mentioned above. They include 1-D, 2-D, and 3-D data and also spectral and Doppler information (using range rate or Doppler techniques), polarization, and speckle characteristics. The signal processing for a laser radar is borrowing methods and procedures from conventional radar (see, e.g., [96, 97]) and conventional image processing [see, e.g., 98]. Spectral processing can rely on the manifold of methods developed for hyperspectral imaging [see, e.g., 99].

The additional issues for laser radar processing with respect to microwave radar involve different target and background characteristics, detection in photon noise, atmospheric propagation effects (attenuation, scattering, and turbulence), and the issue of angular resolved targets.

In relation to conventional image processing, the ladar often adds complexity but also new opportunities due to speckles, scintillation, and high-range resolution, which enables range segmentation and 3-D matching, for example.

As the subject of signal and image processing is vast, we will just give a few examples of recent signal handling in active imaging and mapping.

In mapping, the processing of individual laser waveforms is essential to extract as much information as possible. In a review paper, Guenther et al. [100] describe hardware and software design philosophy including signal processing issues together with the historic development of airborne lidar bathymetry. Recent work in airborne bathymetric waveform processing in combination with satellite data for seafloor classification has been presented by Tulldahl et al. [101]. A summary of the methods and processing used for forest inventory can be read in the paper by Hyyppä et al. [42].

The capability of 3-D ladars looking through vegetation in a single or by multiple looks is attractive for both airborne and ground-to-ground applications. Proper processing of 3-D data will give a good opportunity to reveal targets hidden in vegetation. Examples of such processing were discussed in relation to Figure 5 [34, 35]. Cho et al. [102] at MIT describes a prototype image processing system, which generates, displays, and analyzes 3-D ladar data from single photon detection in real time. The system also discriminates static from dynamic objects in a scene. A new and improved algorithm for noise removal and signal detection in 3-D ladar imagery, called multiple-peak spatial coincidence processing (MPSCP), is presented by Vasile et al. [103].

Grönwall and Tolt [104] propose a target segmentation approach based on sensor data fusion that can deal with the problem of a diverse background. Features from sensor images, including data from a laser scanner and passive sensors (cameras), are analyzed using Gaussian mixture estimation.

Armbruster [105] gives examples of 3-D laser radar applications, for which automatic data processing can exceed human visual cognition capabilities and describes basic processing techniques for attaining these results. The examples are drawn from the fields of helicopter obstacle avoidance, object detection in surveillance applications, model-based object recognition in single range images, multi-object tracking, and object recognition in range image sequences. The techniques are based on Bayesian decision-theoretic foundations, guaranteeing optimal ATR solutions both for single images and range image sequences. In recent papers, Armbruster et al. investigate flash ladar data from maritime targets concerning segmentation, classification, identification, and pose estimation [106, 107].

Future challenges in active spectral imaging involve efficient data fusion methods combining ladar features such as 3-D shape and intensity with spectral characteristics. These techniques have been studied in mapping for some years (see, e.g., [108, 109]). For defense and security, new opportunities and challenges involve space time (4-D) processing for robust detection, tracking, and recognition.

6 Discussion

In this paper, we have tried to review active imaging with emphasis on discussing the benefit of adding the spectral domain either as a passive sensor or as a multi- or hyperspectral laser. The combination of a fix wavelength laser and a spectral passive sensor is a rather well-established technique especially in remote sensing mapping systems. Some drawbacks with this method is the problem of aligning two separate sensors with often different pixel sizes and also the fact that the sensor may have different penetration capabilities through shadows, water, and other obscurants. Active multi- or hyperspectral sensors avoid these problems and also offer the possibility of absolute measurements as they have full control of the illumination.

One of the main limitations in active spectral imaging is the technology limitations for efficient and powerful multiline or tunable lasers. There is also an increased complexity for the receiver, which must have a spectral discrimination either through fixed or tunable filters. Other solutions may involve transforming the spectral domain to time [84] or using a streak camera, the so-called multislit STIL [36].

Although supercontinuum laser are quite promising, the splitting into too many spectral channels will lower the sensitivity of the system. On the other hand, the advances or sensitive receivers based on single photon counting may allow for that.

However, the potential advantages in active spectral imaging are many, and we can foresee new applications and capabilities in such areas as remote sensing of the terrain (tree and plant classification, plant conditions, and others), ocean monitoring (suspended and dissolved matter, bottom classification, etc.), as well as detection of aerosols and gases on the atmosphere. In the security and defense area, we note stand-off detection of dangerous substances (CBRNE), improved target detection and classification including material classification, effluent and trace detection, as well as other applications.

Concerning the future system development for active spectral imaging and mapping, the fix frequency lidar and a multi- or hyperspectral passive sensor will probably be dominating at least for a foreseeable future. The fix or few wavelength lidar can generate enough power to enable long-range applications (km). This type of laser can excite spectral emission in gases and solids, which can be detected at remote distances. However, a true active spectral imaging/mapping system with multi-wavelength or continuous emission will find applications when sensitive detectors and compact powerful sources allow cost-effective sensors to be built.

Acknowledgments: The work and examples referring to the Swedish Research Agency (FOI) have been supported by the Swedish Armed Forces, the Swedish Defense Material Administration (FMV), and the European Defense Agency (EDA).

Received December 20, 2013; accepted January 20, 2014; previously published online February 28, 2014

References

[1] P. F. McManamon, Opt. Eng. 51, 060901 (2012).
[2] O. Steinvall, Proc. SPIE 5989, 598903 (2005).
[3] V. Molebny, G. Kamerman and O. Steinvall, Proc. SPIE 8037, 803709 (2011).
[4] V. Molebny, G. Kamerman and O. Steinvall, Proc. SPIE 7835, 783502 (2010).
[5] V. A. Kovalev and W. E. Eichinger, 'Elastic Lidar', (John Wiley and Sons, 2004), ISBN 0-471-20171-5.
[6] The Infrared and Electro-Optical Systems Handbook, Vol. 6. Active Electro-Optical Systems, Society of Photo-Optical Engineers, 90, (1993).
[7] D. L Hutt, J. M Theriault, V. G. Larochelle, P. Mathieu and D. Bonnier, Opt. Eng. 33, 3762–3773 (1994).
[8] T. Kaurila, A. Hågård and R. Persson, Appl. Opt. 45, 6750–6761 (2006).
[9] R. M. Corless, G. H. Gonnet, D. E. G. Hare, D. J. Jeffrey and D. E. Knuth, Adv. Comput. Math. 5, 329–359 (1996).
[10] O. Steinvall, Appl. Opt. 48, B1–B7 (2009).
[11] R. R. Rupp, Z. Derzko and G. R. Ax, Jr., Proc. SPIE 5415, 1151–1161 (2004).
[12] ASTAMIDS, http://www.gizmodo.com.au/2012/05/astamids-fly-by-mine-detectors-save-us-lives-and-limbs/.
[13] Sensors unlimited, http://www.sensorsinc.com/swirconops.html.
[14] QPC lasers, http://www.qpclasers.com/.
[15] Pranalytica, http://www.pranalytica.com/products-services/downloads.php.
[16] L. Goldberg, J. Leach, S. Chinn and V. King, Proc. SPIE 8605, 860512 (2013).
[17] P. Andersson, Opt. Eng. 45, 034301 (2006).
[18] O. Steinvall, M. Elmqvist, T. Chevalier and O. Gustafsson, Appl. Opt. 52, 4763–4778 (2013).
[19] General Photonics, http://www.ga-asi.com/products/sensor_systems/spi3d.php.
[20] Thales Group, http://www.thalesgroup.com/Portfolio/Aerospace/DAMOCLES_Targeting_pod/?pid=1498.
[21] http://www.selexsas.com/EN/Common/files/SELEX_Galileo/Products/PicoSTAR.pdf.
[22] http://www.obzerv.com/night-vision-cameras/.
[23] O. David, R. Schneider and R. Israeli, Proc. SPIE 7482, 748203 (2009).
[24] Z. Xiuda, Y. Huimin and J. Yanbing, Opt. Lett. 33, 1219–1221 (2008).
[25] M. Laurenzis, F. Christnacher, N. Metzger, E. Bacher and I. Zielenski, Proc. SPIE, 7298, 729833-1 (2009).
[26] M. Laurenzis, Appl. Opt. 49, 2271–2276 (2010).
[27] E. de Borniol, F. Guellec, J. Rothman, A. Perez, J.-P. Zanatta, et al., Proc. SPIE 7660, (2010).
[28] A. Ashcroft and I. Baker, Proc. SPIE 7660, (2010).
[29] Goodrich Sensors Unlim. Inc., www.sensorsinc.com/.
[30] XenICs nv, http://www.xenics.com/.
[31] Raptor Photonics, http://www.raptorphotonics.
[32] Intevac Inc., http://intevac.com/.
[33] M. Vaidyanathan, S. Blask, T. Higgins, W. Clifton, D. Davidhson et al., Proc. SPIE 6550, Laser Radar Technology and Applications XII, pp. 65500N (2007).
[34] M. Marino Richard and William R. Davis, Jr., LLabJ. 15, 23–36 (2005).
[35] C. Grönwall, G. Tolt, T. Chevalier and H. Larsson, Opt. Eng. 50, 047201 (2011).

[36] Arete, http://www.arete.com/arete_innovation/multislit_stil.aspx.
[37] Prinecton Lightwave, http://www.princetonlightwave.com/mm-products/3d-ladar.
[38] M. Jack, J. Wehner, J. Edwards and G. Chapman, Proc. SPIE, 8033, 80330M, (2011).
[39] J. Shan and C. K. Toth, Topograhic Laser Ranging and Scanning – Principles and Processing (CRC Press, 2009).
[40] A. Nayegandhi, J. C. Brock and C. Wayne Wright, ASPRS 2005 Annual Conference "Geospatial Goes Global: From Your Neighborhood to the Whole Planet", March 7–11, (2005).
[41] https://lvis.gsfc.nasa.gov/index.php.
[42] J. Hyyppä, H. Hyyppä, D. Leckie, F. Gougeon, X. Yu, et al., Int. J. Remote. Sens. 29, 1339–1366 (2008).
[43] www.opentopography.org/index.php/blog/detail/a_quick_look_at_nga_lidar_from_haiti/.
[44] http://www.reuters.com/article/2011/04/27/idUS280475+27-Apr-2011+MW20110427.
[45] www.sigmaspace.com/sigma/3DImagingLidars.php.
[46] J. Degnan, R. Machan, E. Leventhal, D. Lawrence, G. odor, et al., Proc. SPIE, 6950, 695007 (2008).
[47] http://www.darpa.mil/grandchallenge/index.asp.
[48] O. Steinvall, I. Renhorn, J. Ahlberg, H. Larsson, D. Letalick, et al., Proc. SPIE, 7835, 78350C, SPIE Europe Security and Defence 2010, Toulouse (2010).
[49] D. Hamoir, L. Hespel, Y. Bouchera, P. Déliot, O. Steinvall, Proc. SPIE, 8186, 81860M (2011).
[50] K. Lewis, Proc. SPIE, 8868, 88680Q (2013).
[51] E. Repasi, P. Lutzmann, O.Steinvall, M. Elmqvist, B. Göhler, et al., Appl. Opt. 48, 5959–5969 (2009).
[52] M. L. Nischan, R. M. Joseph, J. C. Libby and J. P. Kerekes, LLabJ. 14, 131–144 (2003).
[53] L. Farr, M. Watson and G Bishop, "Active Spectral Imaging for Target Detection" BAE SYSTEMS Advanced Technology Centre Filton, Bristol, BS34 7QW, 3rd EMRS DTC Technical Conference – Edinburgh (2006).
[54] G. Bishop, I Vallejo Veiga, M Watson and L. Farr, Active Spectral Imaging for Target Detection" BAE SYSTEMS Advanced Technology Centre Filton, Bristol, BS34 7QW. 4th EMRS DTC Technical Conference – Edinburgh (2007).
[55] M. Alouini, F. Goudail, A. Grisard, J. Bourderionnet, D. Dolfi, et al., Appl. Opt. 48, 1610–1618 (2009).
[56] B. Kinder, J. P. Garcia, R. D. Habbit and E. L. Dereniak, Proc. SPIE 5159, 73–81 (2003).
[57] Y. Wang, Y. Wang and H. Q. Lea, Opt. Exp. 13, 6572–6586 (2005).
[58] C. Hardie, M. Vaidyanathan and P. F. McManamon, Opt. Eng. 37, 752–762 (1998).
[59] J.-R. Simard, P. Mathieu, G. Fournier and V. Larochelle, Proc. SPIE 4035, 180–191 (2000).
[60] J. F. Andersen, J. Busck and H. Heiselberg, Appl. Opt. 45, 6198–6208 (2006).
[61] M. A. Powers and C. C. Davis, Proc. SPIE 7324, 7324OU 1–11 (2009).
[62] M. A. Powers and C. C. Davis, Appl. Opt. 51, 1468–1478 (2012).
[63] J. M. Cathcart, J. T. Harrell and T. West, Proc. SPIE 6538, 65381N, (2007).
[64] D. J. M. Stothard, M. H. Dunn and C. F. Rae, Opt. Expr. 12, 947–955 (2004).
[65] C. R. Howle, D. J. M. Stothard, C. F. Rae, M. Ross, B.S. Triscott, et al., Proc. SPIE, 6954, 69540L-1-12 (2008).
[66] K. Ruxton, G. Robertson, B. Miller, G. P. A. Malcolm and G. T. Maker, Proc. SPIE 8710, 87100L (2013).
[67] R. J. Clewesa, C. R. Howlea, J. Guicheteaub, D. Emge, K. Ruxton, et al., Proc. SPIE 8710, 871002 (2013).
[68] S. Wallin, A. Pettersson, H. Ostmark and A. Hobro, Anal. Bioanal. Chem. 395, 259–274 (2009).
[69] A. Pettersson, S. Wallin, H. Östmark, A. Ehlerding, I. Johansson, et al., "Explosives standoff detection using Raman spectroscopy: From bulk towards trace detection", Proc. of SPIE Vol. 7664, (2010).
[70] H. Östmark, M. Nordberg and T. E. Carlsson, "Stand-off detection of explosives by multispectral imagin Raman spectroscopy", Allied Optics, Vol. 50, No. 28, (2011).
[71] L. A. Skvortsov, Quant. Elect. 41, 1051–1060 (2011).
[72] A. K. Goyal, M. Spencer, M. Kelly and J. Costa, Proc. SPIE 8018, 80180N (2011).
[73] C. Bauer, U. Willer and W. Schade, Opt. Eng. 49, 111126 (2010).
[74] R. Furstenberg, M. Papantonakis, C. A. Kendziora, D. M. Bubb, J. Corgan, et al., Proc. SPIE 7665, 76650Q (2010).
[75] F. Fuchs, S. Hugger, M. Kinzer, B. Hinkov, R. Aidam, et al., Proc. SPIE 7808, 780810 (2010).
[76] F. Fuchs, S. Hugger, M. Kinzer, R. Aidam, W. Bronner, et al., Opt. Eng. 49, 111127 (2010).
[77] O. Steinvall, I. Renhorn and D. Letalick, Proc. SPIE 7114, 711407 (2008).
[78] A. L. Schneider, D. Monnin, M. Laurenzis and F. Christnacher, Proc. SPIE 8897, 88970L (2013).
[79] C. Grönwall, D. Hamoir, O. Steinvall, H. Larsson, E. Amselem, et al., Proc. SPIE 8897, 889705 (2013).
[80] V. Farley, M. Kastek, M. Chamberland, T. Piątkowski, P. Lagueux, et al., Proc. SPIE 8743, 87431P (2013).
[81] P. Zhou, F. Wang, H. Zhang and M. Xue, Proc. SPIE 8194, 81940Y (2011).
[82] M. A. Hogervorst, A. Toet and P. Jacobs, Proc. SPIE 7662, 766205 (2010).
[83] R. A. Lamb, Proc. SPIE 7483, 748308 (2009).
[84] K. Goda, K. K. Tsia and B. Jalali, Nature, 45, 07980 (2009).
[85] I. H. Woodhouse, C. Nichol, P. Sinclair, J. Jack, F. Morsdorf, et al., IEEE Geosci. Remote. Sens. Lett. 8, 839–843 (2011).
[86] F. Morsdorf, C. Nichol, T. Malthus and I. H. Woodhouse, Remote Sens Environ. 113, 2152–2163 (2009).
[87] J. Jack, E. Rumi, D. Henry, I. Woodhouse, C. Nichol, et al., Proc. SPIE 8176, 81761O (2011).
[88] T. Hakala, J. Suomalainen, S. Kaasalainen and Y. Chen, Opt. Exp. 20, 7119–7127 (2012).
[89] Y. I. Kopilevich and V. I. Feigels, Ocean Optics: Remote Sensing and Underwater Imaging, 51 (2002).
[90] H. M. Tulldahl, P. Philipson, H. Kautsky and S. A. Wikström, Proc. SPIE 8724, 87240B (2013).
[91] O. Steinvall, H. Kautsky, M. Tulldahl and E. Wollner, Proc. SPIE. 8724, Ocean Sensing and Monitoring V 87240B (2013).
[92] O. Friman, G. Tolt and J. Ahlberg, Proceedings of SPIE Remote Sensing 2011, Paper 8180-26, Prague, Czech Republic, FOI-S--3939--SE (2011).
[93] G. Tolt, M. Shimoni and J. Ahlberg, 4423–4426, FOI-S–3960–SE (2011).
[94] M. Shimoni, G. Tolt, C. Perneel and J. Ahlberg, Proceedings of the IEEE International Geoscience and Remote Sensing

Symposium (IGARSS), Vancouver, Canada, 4427–4430, FOI-S–3961–SE (2011).
[95] V. I. Feygels, J. Y. Park, J. Wozencraft, J. Aitken, C. Macon, et al., Proc. SPIE 8724, 87240A (2013).
[96] M. A. Richards, 'Fundamentals of Radar Signal Processing', (McGraw-Hill, New York, 2005).
[97] M. I. Skolnik, 'Radar Handbook', 2nd ed. (McGraw-Hill, New York, 1990).
[98] W. K. Pratt, in 'Introduction to Digital Image Processing', (CRC Press, Boca Raton, FL, USA, 2013).
[99] M. Eismann, in 'Hyperspectral Remote Sensing', (SPIE Press, Belligham, Washington, USA, 2012).
[100] G. C. Guenther, A. G. Cunningham, P. E. LaRocque and D. J. Reid, Proceedings of EARSeL-SIG-Workshop LIDAR, Dresden/FRG, June 16–17, (2000).
[101] H. M. Tulldahl and S. A. Wikström, Remote Sens Environ. 121, 347–357 (2012).
[102] P. Cho, H. Anderson, R. Hatch and P. Ramaswam, LlabJ. 16, 1 (2006).
[103] A. N. Vasile, L. J. Skelly, M. E. O'Brien, D. G. Fouche, R. M. Marino, et al., Adv. Visual Comput. Lect. Notes Compu. Sci. 7431, 382–393 (2012).
[104] C. Grönwall and G. Tolt, Proc. 17th Scandinavian Conference on Image Analysis (SCIA2011), Ystad, May 23–27, (2011), pp. 708–718.
[105] W. Armbruster, International Symposium Photoelectronic Detection and Imaging (Beijing, China, 2009).
[106] W. Armbruster, M. Hammer, Proc. SPIE 8542, 85420K (2012).
[107] W. Armbruster, M. Hammer, Proc. SPIE 8391, 83910C (2012).
[108] M. Dalponte, L. Bruzzone and D. Gianelle, IEEE Trans. Geosci. Remote Sens 46, 1416–1427 (2008).
[109] S. C. Popescu and R. H. Wynne, Photogramm Eng Rem S 70, 589–604 (2004).

Ove Steinvall received his MS degree in Physics at the University of Uppsala in 1969. He was then employed by the National Defence Res. Establishment (FOA, now FOI) in 1969. He received his PhD in 1974 from the Chalmers Institute of Technology in Lasers and Electro-Optics. Since 1977, he has been leading the Laser group, from 1994 as a Department Head and from 2007 as head of the Optronic Systems Department, and currently as a research director. His research activities include lasers, lasers for countermeasures, laser warning, laser radar/lidar including systems for imaging and mapping, free space laser communications and ocean /atmospheric optics. He is author or coauthor of about 100 conference and journal articles and approximately 300 internal reports. Dr. Steinvall is a fellow of the Society for Photo-Optical Instrumentation Engineers (SPIE), and a member of the Optical Society of America, the Swedish Optical Society, and the Royal Academy of Military Sciences. He has received three national awards for his laser work. He has also received the NATO Scientific Achievement Award (SET-077). He has been the conference chair for several laser conferences. He is an expert in EDA Captech IAP3 and holds a position as Assistant Professor at the Chalmers Institute of Technology.